京都大学防災研究所年報 第 54 号 B 平成 23 年 6 月
Annuals of Disas. Prev. Res. Inst., Kyoto Univ., No. 54 B, 2011

Experimental and Numerical Study of Rainfall Induced Slope Failure

Ram Krishna REGMI*, Hajime NAKAGAWA, Kenji KAWAIKE, Yasuyuki BABA and Hao ZHANG

* Department of Civil and Earth Resources Engineering, Kyoto University

Synopsis

The purpose of this study was to predict the failure surface of a slope due to rainfall. Numerical and experimental study was performed to investigate the mechanism of the slope failure. Slope stability analysis was carried out in three dimensions using the pore water pressure and the moisture content calculated by three dimensional seepage flow model. Only a conventional water-phase seepage flow model as well as the water-air two-phase seepage flow model, coupled with two dimensional surface flow and erosion/deposition model, were used for seepage analysis. In numerical analysis, the influence of pore air on seepage and slope stability was found to be less significant.

Keywords: seepage analysis, variably saturated soil, slope stability, failure surface

1. Introduction

Slope failures in residual soils are common in many tropical countries particularly during periods of intense rainfall. The location of the groundwater table in these slopes may be in deep below the ground surface and the pore-water pressures in the soil above the groundwater table are negative to atmospheric conditions. This negative pore-water pressure, referred to as matric suction when referenced to the pore-air pressure that contributes towards the stability of unsaturated soil slopes (Fredlund and Rahardjo, 1993; Rahardjo et al., 1995; Griffiths and Lu, 2005). Under the influence of rainfall infiltration, water seepage can cause a gradual loss of matric suction in an unsaturated soil slope. As the hydraulic properties of the soil with respect to matric suction are often highly nonlinear, rapid changes in pore-water pressure have a significant effect on the soil strength, and therefore on the stability of the slope.

Rainfall-induced slope failures are generally caused by increased pore pressures and seepage forces during periods of intense rainfall (Terzaghi 1950; Sidle and Swanston 1982; Sitar et al. 1992; Anderson and Sitar 1995; Wang and Sassa 2003). The effective stress in the soil will be decreased due to the increased pore pressure and thus reduces the soil shear strength, eventually resulting in slope failure (Brand 1981; Brenner et al. 1985). In tropical areas, slope failures due to rainfall infiltration are quite usual. These slopes remain stable for a long time before the rainstorms (Brand 1984; Toll 2001). During the rainfall, a wetting front goes deeper into the slope, resulting in a gradual increase of the water content and a decrease of the negative pore-water pressure. This negative pore-water pressure is referred to as matric suction when referenced to the pore air pressure that contributes towards the stability of unsaturated soil slopes. The loss of suction causes a decrease in shear strength of the soil on the potential failure surface and finally triggers the failure (Rahardjo et al. 1995; Ng and Shi 1998).

During intense rainfall events the variations in pore water pressures distributed within the soil are highly variable depending on the hydraulic conductivity, topography, degree of weathering, and fracturing of the soil. Pore water pressure increases may be directly related to rainfall infiltration and percolation or may be the result of the build-up of a perched or groundwater table (Terlien, 1998). The response of the material involved is largely dependent on its permeability. In high-permeability soils the build-up and dissipation of positive pore pressures during intense precipitation events could be very rapid (Johnson and Sitar, 1990). In these cases slope failures are caused by high intensity rainfall and antecedent rainfall has little influence on landslide occurrence (Corominas, 2001). On the contrary, in low-permeability soils slope failures are caused by long duration-moderate intensity rainfall events; in fact, the reduction in soil suction and the increase in pore water pressures due to antecedent rainfall, considered a necessary condition for landslide occurrence (Sanderson et al., 1996; Wieczorek, 1987).

Various physically based models coupling the infinite slope stability analysis with the hydrological modeling were developed assuming steady or quasi-steady water table and groundwater flows parallel to hill slope (Montgomery and Dietrich 1994; Wu and Sidle 1995; Borga et al. 1998). With approximation of Richards' equation (1931) valid for hydrological modeling in nearly saturated soil, Iverson (2000) further developed a flexible modeling framework of shallow landslide. Baum et al. (2002) proposed an extension version of Iverson's model to consider variable rainfall intensity into account for hill slope with finite depth. Tsai and Yang (2006) modified Iverson's model by amending the boundary condition at the top of the hill slope to consider more general infiltration process instead of constant infiltration capacity. The physically based model with the hydrological modeling in nearly saturated soil (Iverson 2000; Baum et al. 2002; Tsai and Ynag 2006) was commonly used for the assessment of shallow landslides triggered by rainfall due to its simplicity (Crosta and Frattini 2003; Keim and Skaugset 2003; Frattini et al. 2004; Lan et al. 2005; D'Odorico et al. 2005; Tsai 2007). Tsai et al. (2008) developed a physically based model not only by using the complete Richards' equation with the effect of slope angle, but also by adopting the extended Mohr-Coulomb failure criterion (Fredlund et al. 1978) to describe the unsaturated shear strength.

Sassa (1972, 1974) carried out a series of flume tests and concluded that the changes in rigidity of sand and upper yield strain within a slope are essential to the analysis of slope stability. Fukuzono (1987) conducted experiment to examine the conditions leading up to slope failure using nearly actual-scale slope models providing heavy rainfall. Crozier (1999) tested a rainfall-based landslide-triggering model developed from previous landslide episodes in Wellington City, NewZealand, which referred to as the Antecedent Water Status Model, to provide a potentially useful level of prediction of landslide occurrence by providing a 24-hour forecast. Sharma (2006) carried out experimental and numerical studies to investigate effects of slope angle on the moisture movement on unsaturated soil and further on the slope stability, and also analyzed the difference in failure pattern and moisture movement in single and two layers of soil with different hydraulic conductivities. Tsustumi and Fujita (2008) investigated several landslide sites and used physical experiment and numerical simulation with the combination of rainwater infiltration for the analysis of slope stability. Mukhlisin and Taha (2009) developed numerical model to estimate the extent of rainwater infiltration into an unsaturated slope, the formation of a saturated zone, and the change in slope stability. Then, the model was used to analyze the effects of soil thickness on the occurrence of slope failure.

The above discussed numerical studies are applicable only for two dimensional analyses; however failure of slopes occurs in three dimensions. There is not only water phase but also air phase in soil slopes. Both the pore air and pore water will have influence on the seepage flow, but all the above mentioned studies have neglected the air flow on seepage analysis. In looking at the behaviour of unsaturated soils, some authors (e.g. Dakshanamurthy et al, 1984) incorporate airflow within the soil, and it is clear that this aspect can be significant to the overall behaviour of the soil.

Therefore, numerical study in three dimensions is necessary for seepage analysis and slope stability analysis with considering the effects of air phase in the seepage.

In this study the analysis of slope failure due to rainfall was investigated using pore water pressure and moisture content calculated by only a conventional water-phase seepage flow model as well as the water-air two-phase seepage flow model. Janbu's simplified method was incorporated into dynamic programming to locate the critical slip surface of a general slope. Simulation results were compared with the experimental results obtained so as to evaluate the capability of the model.

2. Numerical Modeling

Numerical models can be valuable tools in the prediction of seepage and the slope stability analysis. In the present analysis single-phase seepage flow model calculates the pore water pressure and moisture content inside the body of the considered model slope where as the two-phase model calculates the pore water pressure, pore air pressure, and moisture content. Necessary surface water head for the seepage flow model was evaluated using surface flow and erosion/deposition model. Slope stability model uses the pore water pressure and moisture content obtained by the seepage flow model as well as surface water head obtained by the surface flow and erosion/deposition model as in put data to calculate the critical slip surface and the corresponding factor of safety simultaneously.

2.1 Seepage flow model

Following pressure based Richards' equation valid for variably saturated soil was used in conventional 3D seepage flow model for calculating the change in pore water pressure inside the model slope (Awal et al., 2009).

$$\left(C + S_w S_s\right)\frac{\partial h_w}{\partial t} = \frac{\partial}{\partial x}\left(K_x \frac{\partial h_w}{\partial x}\right) + \frac{\partial}{\partial y}\left(K_y \frac{\partial h_w}{\partial y}\right) + \frac{\partial}{\partial z}\left(K_z\left(\frac{\partial h_w}{\partial z} + 1\right)\right) \quad (1)$$

where, h_w is the water pressure head; K_x, K_y and K_z are the hydraulic conductivity in x, y and z direction respectivel; $C=\partial\theta_w/\partial h_w$ is the specific moisture capacity, θ_w is the soil volumetric water content; S_w is the saturation ratio; S_s is the specific storage; t is the time; x and y are the horizontal spatial coordinates; and z is the vertical spatial coordinate taken as positive upwards.

In order to solve the equation (1) following constitutive relationships proposed by van Genuchten (1980) are used for establishing relationship of moisture content and water pressure head (θ_w-h), and unsaturated hydraulic conductivity and moisture content(K-θ_w):

$$S_e = [1 + (|\alpha h_w|)^{\eta}]^{-m} \quad (2)$$

$$S_e = \frac{\theta_w - \theta_r}{\theta_s - \theta_r} \quad (3)$$

$$K = K_s S_e^{0.5}[1 - (1 - S_e^{1/m})^m]^2 \quad (4)$$

where, S_e is the effective saturation; α and η are empirical parameters; θ_s and θ_r are saturated and residual moisture content respectively; K_s is the saturated hydraulic conductivity; and $m=1-1/\eta$.

For 3D water-air two-phase seepage flow analysis, following equations are derived for the simultaneous flow of water and air based on the 1D flow equations (Touma, and Vauclin, 1986).

Water-phase equation

$$C\left(\frac{\partial h_a}{\partial t} - \frac{\partial h_w}{\partial t}\right) = \frac{\partial}{\partial x}\left(K_{wx}\frac{\partial h_w}{\partial x}\right) + \frac{\partial}{\partial y}\left(K_{wy}\frac{\partial h_w}{\partial y}\right) + \frac{\partial}{\partial z}\left(K_{wz}\left(\frac{\partial h_w}{\partial z} + 1\right)\right) \quad (5)$$

Air-phase equation

$$\left(\left(n - \theta_w\right)\frac{\rho_{oa}}{h_o} - \rho_a C\right)\frac{\partial h_a}{\partial t} + \rho_a C\frac{\partial h_w}{\partial t} = \frac{\partial}{\partial x}\left(\rho_a K_{ax}\frac{\partial h_a}{\partial x}\right) + \frac{\partial}{\partial y}\left(\rho_a K_{ay}\frac{\partial h_a}{\partial y}\right) + \frac{\partial}{\partial z}\left(\rho_a K_{az}\left(\frac{\partial h_a}{\partial z} + \frac{\rho_a}{\rho_{ow}}\right)\right) \quad (6)$$

where, h_a is the air pressure head; h_o is the atmospheric pressure expressed in terms of water column height; $C= \partial\theta/\partial h_c$ is the specific moisture capacity; $h_c = h_a - h_w$ is capillary head; n is the porosity of soil; ρ_a is density of air; ρ_{oa} is density of

air at the atmospheric pressure; ρ_{ow} is density of water at the atmospheric pressure; K_{wx}, K_{wy} and K_{wz} are the hydraulic conductivity in x, y and z directions respectively; and K_{ax}, K_{ay} and K_{az} are the air conductivity in x, y and z directions respectively.

In order to solve the equations (5) and (6) following constitutive relationships proposed by van Genuchten (1980) are used:

$$S_e = [1 + (\alpha h_c)^{\eta}]^{-m} \tag{7}$$

$$S_e = \frac{\theta_w - \theta_r}{\theta_s - \theta_r} \tag{8}$$

$$K_w = K_{ws} S_e^{0.5} [1 - (1 - S_e^{1/m})^m]^2 \tag{9}$$

$$K_a = K_{as} (1 - S_e)^{0.5} [(1 - S_e^{1/m})]^{2m} \tag{10}$$

where, K_{ws} is the saturated hydraulic conductivity; $K_{as}=K_{ws}$ (μ_w/μ_a) is the saturated air conductivity; and μ_w and μ_a are dynamic viscosity of water and air respectively. $\mu_w = 1.002\times10^{-2}$ NS/m^2 and $\mu_a = 1.83\times10\text{-}5$ NS/m^2 at $20°c$.

Numbers of methods are available for the numerical solution. In several 1D variably saturated flow studies, finite difference schemes have been widely used (e.g. Day and Luthin, 1956; Freeze, 1969; Kirkby, 1978; Dam and Feddes 2000; Vasconcellos and Amorim, 2001). However, fewer researchers have used finite differences to solve variably saturated flow problems in higher dimensions. In this study, the equations (1), (5) and (6) are solved by line successive over relaxation (LSOR) scheme used by Freeze (1971a, 1971b, 1978) by an implicit iterative finite difference scheme.

2.2 Surface flow and erosion/deposition model

The mathematical model developed by Takahashi and Nakagawa (1994) was used to investigate the surface flow and erosion/deposition on the surface of the model slope. The depth-wise averaged two-dimensional momentum equations for the x-wise (down valley) and y-wise (lateral) directions are:

$$\frac{\partial M}{\partial t} + \beta \frac{\partial (uM)}{\partial x} + \beta \frac{\partial (vM)}{\partial y} = gh \sin\theta_{bxo} - gh\cos\theta_{bxo} \frac{\partial (h + z_b)}{\partial x} - \frac{\tau_{bx}}{\rho_T} \tag{11}$$

and

$$\frac{\partial N}{\partial t} + \beta \frac{\partial (uN)}{\partial x} + \beta \frac{\partial (vN)}{\partial y} = gh \sin\theta_{byo} - gh\cos\theta_{byo} \frac{\partial (h + z_b)}{\partial y} - \frac{\tau_{by}}{\rho_T} \tag{12}$$

The continuity of the total volume is

$$\frac{\partial h}{\partial t} + \frac{\partial M}{\partial x} + \frac{\partial N}{\partial y} = i_b \{c_* + (1 - c_*) s_b\} + R - I \tag{13}$$

The continuity equation of the particle fraction is

$$\frac{\partial (ch)}{\partial t} + \frac{\partial (cM)}{\partial x} + \frac{\partial (cN)}{\partial y} = i_b c_* \tag{14}$$

The equation for the change of bed surface elevation is

$$\frac{\partial z_b}{\partial t} = -i_b \tag{15}$$

where, M $(=uh)$ and N $(=vh)$ are the flow discharge per unit width in x and y directions; u and v are depth averaged velocities in x and y directions; h is the water depth; g is the gravitational acceleration; β is the momentum correction factor; ρ_T is the mixture density; τ_{bx} and τ_{by} are the bottom shear stresses in x and y directions; R is the rainfall intensity; I is the infiltration rate; s_b is the degree of saturation in the bed; i_b is the rate of hydraulic erosion or deposition from the flowing water; c is the sediment concentration in the flow; c_* is the maximum sediment concentration in the bed; and z_b is the erosion or deposition thickness measured from the original bed elevation.

Takahashi (1991) categorized the flow as: a) stony debris flow ($c \geq 0.4c_*$), b) immature debris flow ($0.4c_* > c \geq 0.1c_*$) and c) turbulent flow ($c < 0.1c_*$); based on sediment concentration in the flow and proposed different flow resistance equations for each types of flow.

For stony debris flow

$$\tau_{bx} = \frac{1}{8}\left(\frac{d_m}{h}\right)^2 \sigma \lambda^2 u\sqrt{u^2 + v^2} = \frac{\rho_T}{8}\left(\frac{d_m}{h}\right)^2 \frac{u\sqrt{u^2 + v^2}}{\{c + (1-c)\rho/\sigma\}\{(c_*/c)^{1/3} - 1\}^2} \tag{16}$$

$$\tau_{by}=\frac{1}{8}\left(\frac{d_m}{h}\right)^2\sigma\lambda^2 u\sqrt{u^2+v^2}= \frac{\rho_T}{8}\left(\frac{d_m}{h}\right)^2\frac{v\sqrt{u^2+v^2}}{\{c+(1-c)\rho/\sigma\}\{(c_*/c)^{1/3}-1\}^2} \quad (17)$$

For immature debris flow

$$\tau_{bx}=\frac{\rho_T}{0.49}\left(\frac{d_m}{h}\right)^2 u\sqrt{u^2+v^2} \quad (18)$$

$$\tau_{by}=\frac{\rho_T}{0.49}\left(\frac{d_m}{h}\right)^2 v\sqrt{u^2+v^2} \quad (19)$$

For turbulent flow

$$\tau_{bx}=\frac{\rho g n^2 u\sqrt{u^2+v^2}}{h^{1/3}} \quad (20)$$

$$\tau_{by}=\frac{\rho g n^2 v\sqrt{u^2+v^2}}{h^{1/3}} \quad (21)$$

where, n is the Manning's roughness coefficient and dm is the mean diameter of particles.

The erosion velocity for unsaturated bed given by Takahashi (1991) is as follows.

$$\frac{i_b}{\sqrt{gh}}=K_e\sin^{3/2}\theta_b \left\{1-\frac{\sigma-\rho_T}{\rho_T}c\left(\frac{\tan\phi}{\tan\theta}-1\right)\right\}^{1/2} \cdot\left(\frac{\tan\phi}{\tan\theta}-1\right)(c_\infty-c)\frac{h}{d_m} \quad (22)$$

where, ø is the internal friction angle of the bed, K_e is the parameter of erosion velocity and c_∞ is the equilibrium solids concentration. c_∞ is defined by the following equations (Nakagawa et al., 2003).

For stony debris flow (*tanθ>0.138*)

$$c_\infty=\frac{\rho\tan\theta}{(\sigma-\rho)(\tan\phi-\tan\theta)} \quad (23)$$

For immature debris flow (*0.138≥tanθ>0.03*)

$$c_\infty=6.7\left\{\frac{\rho\tan\theta}{(\sigma-\rho)(\tan\phi-\tan\theta)}\right\}^2 \quad (24)$$

For turbulent flow (*0.03≥tanθ*)

$$c_\infty=\frac{(1+5\tan\theta)\tan\theta}{\sigma/\rho-1} \left(1-\alpha_0^2\frac{\tau_{*c}}{\tau_*}\right)\left(1-\alpha_0\sqrt{\frac{\tau_{*c}}{\tau_*}}\right) \quad (25)$$

Where, θ is water surface gradient, and

$$\alpha_0^2=\frac{2\{0.425-(\sigma/\rho)\tan\theta/(\sigma/\rho-1)\}}{1-(\sigma/\rho)\tan\theta/(\sigma/\rho-1)} \quad (26)$$

$$\tau_{*_c}=0.04\times10^{1.72\tan\theta} \quad (27)$$

$$\tau_*=\frac{h\tan\theta}{(\sigma/\rho-1)d_m} \quad (28)$$

in which τ_{*c} is the non-dimensional critical shear stress and τ_* is the non-dimensional shear stress.

If the slope is steeper than about 9 degrees and $c_{s\infty}$ by equation (29) calculates the value less than c_∞

$$c_{s\infty}=6.7c_\infty^2 \quad (29)$$

and for the slope on which $c_{s\infty}$ by equation (29) count less than 0.01, $c_{s\infty}$ should be obtained by using appropriate bed load equation.

The deposition velocity given by Takahashi (1991) is as follows.

$$i_b=\delta_d\frac{c_\infty-c}{c_*}\sqrt{u^2+v^2} \quad (30)$$

where, δ_d is a constant.

The finite difference form of the equations (11) to (14) can be obtained by the solution methods developed by Nakagawa (1989) using Leap-Frog scheme.

2.3 Slope stability model

The stability of a slope depends on its geometry,

soil properties and the forces to which it is subjected to internally and externally. The numerous methods currently available for slope stability analysis provide a procedure for assigning a factor of safety to a given slip surface, but do not consider the problem of identifying the critical conditions. Limit equilibrium method of slices is widely used for slope stability analysis due to its simplicity and applicability. In the method of slices, the soil mass above the slip surface is divided into a number of vertical slices and the equilibrium of each of these slices is considered. The actual number of the slices depends on the slope geometry and soil profile. The limiting equilibrium consideration usually involves two steps; one for the calculation of the factor of safety and the other for locating the most critical slip surface which yields the minimal factor of safety. Methods by Bishop, Janbu, Spencer and Morgenstern and Price are now well known.

In this study Janbu's simplified method has been incorporated into an effective minimization procedure based on dynamic programming by which the minimal factor of safety and the corresponding critical non circular slip surface are determined simultaneously. Fig. 1 shows the three dimensional general slip surface and forces acting on a typical column. W_{ij} is the weight of column; P_{ij} is the vertical external force acting at the top of the column; T_{ij} and N_{ij} are the shear force and total normal force acting on the column base; Q_{ij} is the resultant of all intercolumn forces acting on the column sides; Δx and Δy are discretized widths of the columns in x and y directions respectively; and α_{xz} and α_{yz} are the inclination angles of the column base to the horizontal direction in the xz and yz planes respectively.

The factor of safety F_s for Janbu's simplified method is expressed by the following equation (Awal et al., 2009).

$$F_s = \frac{\sum_{i=1}^{m}\sum_{j=1}^{n}\left[\dfrac{\left(c_e - u_{p_{ij}}\tan\phi\right)\Delta x\Delta y + \left(W_{ij}+P_{ij}\right)\tan\phi}{\left(1/J + \sin\alpha_{xzij}\tan\phi/F_s\right)}\cos\alpha_{xzij}\right]}{\sum_{i=1}^{m}\sum_{j=1}^{n}\left(W_{ij}+P_{ij}\right)\tan\alpha_{xzij}} \quad (31)$$

where, c_e and ϕ are the Mohr-Coulomb strength parameters. $J=(1+\tan2\alpha xzij + \tan2\alpha yzij)1/2$; $W_{ij} = \sum \theta_w(x, y, z, t)\gamma_w dxdydz + \sum c_* \gamma_s dxdydz$ (the weight of a column); $P_{ij} = \sum \gamma_w h(x, y, t)dxdy$ (the vertical external force i.e., surface water weight, acting on the top of the column); $u_{p_{ij}} = Average \sum \gamma_w h_w(x, y, z, t)$ (the pore water pressure at the base of the column) for $h_w(x,y,z,t)>0$; dx, dy and dz are the size of cell used in seepage flow model, γ_w and γ_s are the unit weight of water and solids respectively, c_* is the volume

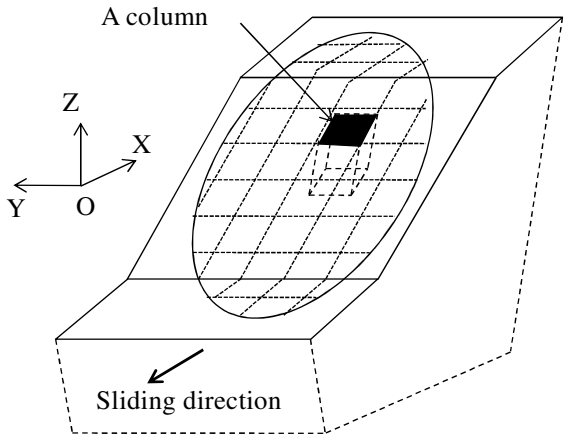

(a) Sliding mass and vertically divided columns

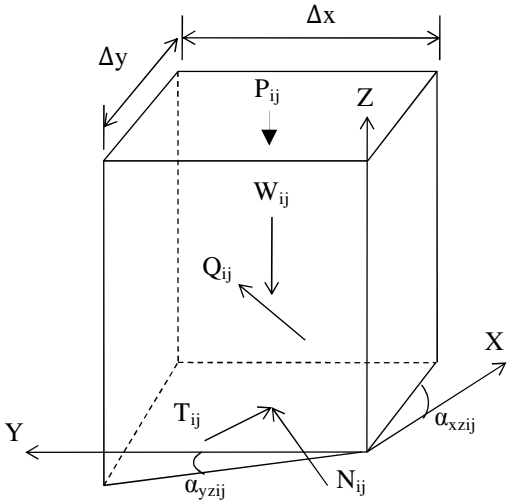

(b) Forces acting on a the column ij

Fig. 1 Three dimensional general slip surface and forces acting on a typical column

concentration of the solids fraction in the body of slope model, $\theta_w(x,y,z,t)$ and $h_w(x,y,z,t)$ are the moisture content and pressure head in each cell and $h(x,y,z,t)$ is the depth of surface water above the cell.

3. Experimental Study

A 3m long, 80cm wide and 70cm deep rectangular flume, with adjustable longitudinal slope was used for the experiment. The flume sidewalls were made of aquarium glass. For capturing the initiation of slope failure process and movement of the failure mass, three digital video cameras (VCs) were used. Two cameras were placed in the sides and one was placed in the front of the flume. The experiments were carried out on 23 degree flume slope. The schematic diagram of the flume, including instrumentation and data acquisition system is shown in Fig. 2.

It is difficult to observe the three dimensional view of the failure surface in rectangular flume shape. So, the rectangular shape of the flume was modified to V-shape having cross slope of 20° by using 292.5 cm long and 3cm thick wooden plates. The downstream end of the flume was closed with a filter mat supported by a wooden plate for retaining the soil and providing downstream free flow condition. The model slope was prepared by placing sediment (Silica sand S6) on the flume and compacted in every 5cm thickness (approximately) using timber plate. A small space was allowed in the upstream for providing runoff input so as to develop water table in the bottom layer of the model slope which is essential for slope failure phenomenon. Profile probes (PRs) consisting four sensors (SRs) were used to measure the temporal variation of moisture content and pressure transducers (PTs) were used to measure the temporal variation of air pressure at different locations inside the body of the model slope.

The flume was in inclined position during the preparation of the model slope for moisture profile and air pressure head profile measurements, whereas it was in horizontal position during the preparation for observing the slope failure process and movement of the failure mass. The profile probes (PRs) and air pressure transducers (PTs) are positioned in their proper location during the preparation of the model slope. Shape and size of the model slope with the arrangement of PRs sensors (SRs) and PTs are schematically shown in Fig. 3.

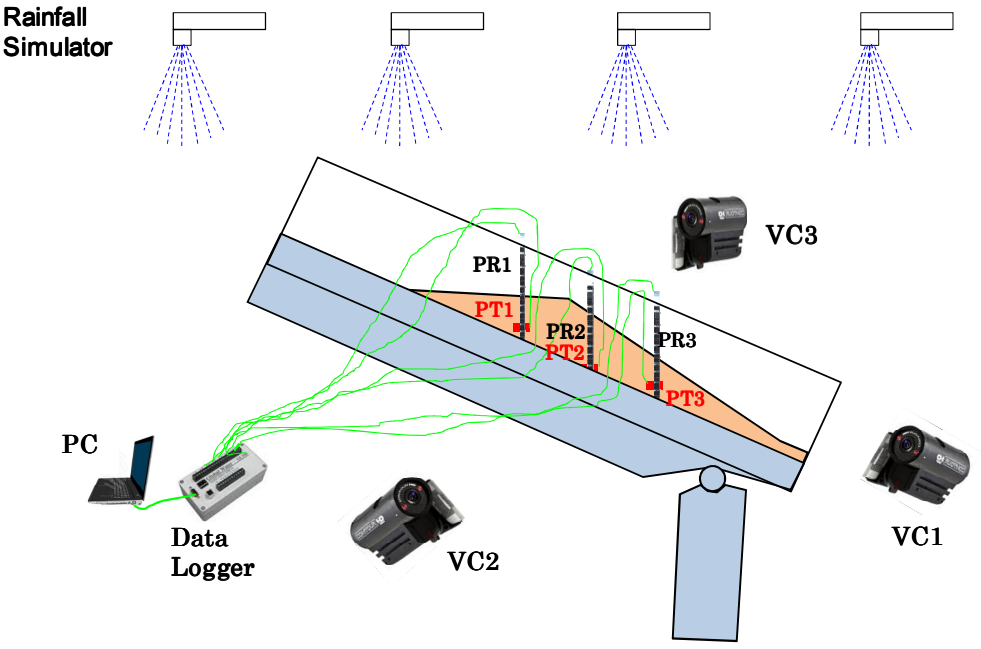

Fig. 2 Experimental setup

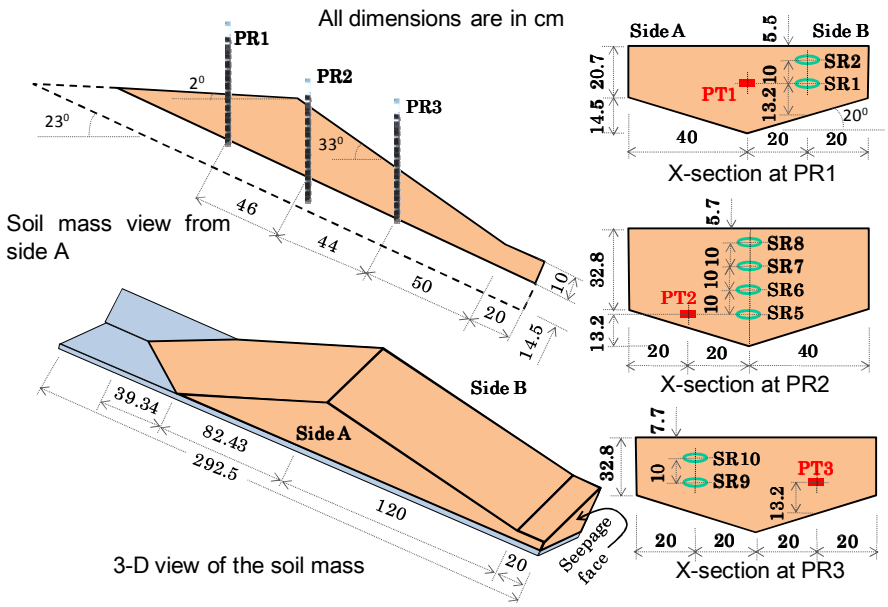

Fig. 3 Shape and size of the model slope with the arrangement of SRs and PTs

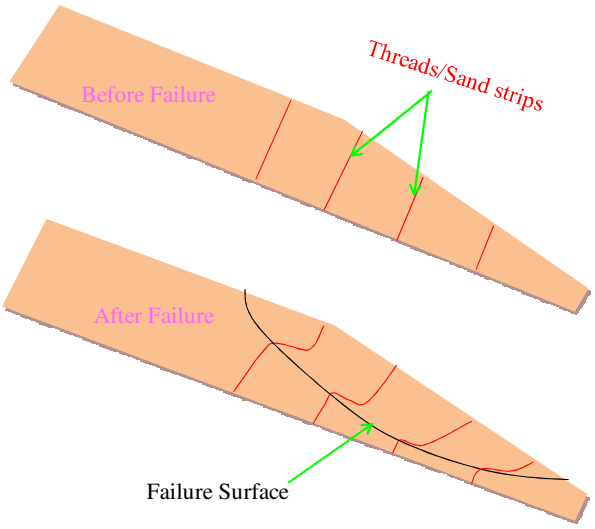

Fig. 4 Typical sketches showing the alignment of threads/sand strips before and after the failure of slope in a particular L-section

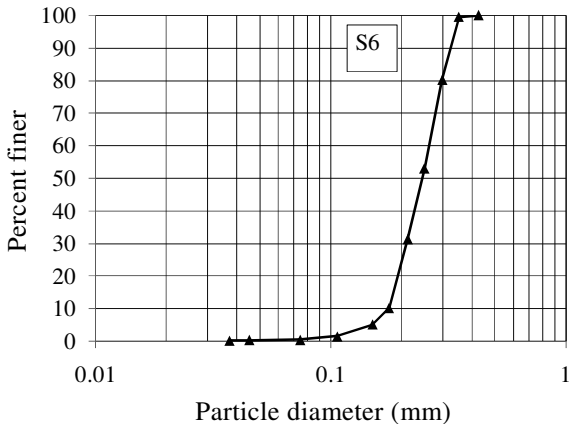

Fig. 5 Grain size distribution of the sediment

Table 1 Some parameter values of the sediment

Sediment type	S6
Saturated moisture content, θ_s	0.42
Residual moisture content, θ_r	0.004
Van Genuchten parameter, α	5.719
Van Genuchten parameter, η	5.044
Specific gravity, G_s	2.63
Mean grain size, D_{50} (mm)	0.24
Angle of repose, ø	34^0
Porosity, n	0.4221
Compression index, CI	1.08

Red colored sediment strips and red colored cotton threads were placed respectively at the side wall faces and inside the body, normal to the flume bed, so as to measure the failure surface after sliding. Sediment strips were placed at the face of the flume and threads were attached firmly in the bottom wall before preparation of the dam body. Fig. 4 presents the typical sketches showing alignment of sand strips/threads before and after the failure of slope in a particular L-section. Some parameter values of the sediment used are listed in Table 1. The grain size distribution of the sediment is shown in Fig. 5.

4. Results and Discussions

Numerical simulation was carried out with time step of 0.01 second and space steps of 2.5cm, 2.424cm and 2.5cm in x (longitudinal), y (lateral) and z (vertical) directions respectively. Both x and y directions were assumed horizontal. In surface water flow and erosion/deposition model, the time step of 0.005sec and space steps of 2.5cm and 2.424cm in x (parallel to longitudinal axis of flume) and y (horizontal) directions respectively. Space steps of 15cm and 10cm in x (parallel to longitudinal axis of flume) and y (horizontal) directions with time step of 10 second was used in slope stability model.

Average rainfall over the flume during experiment was 105.365mm/hr. Fig. 6 shows the rainfall distribution over the flume. In simulation, same rainfall distribution was used. Fig. 7 shows the experimental and simulated air pressure head profiles at the position of different PTs. Fig. 8 shows the experimental and simulated moisture profiles at the position of different SRs.

Essentially air becomes trapped in the voids by the infiltrating water from the surface, initially causing compression of the air phase, leading to a reduction in the rate of water infiltration. The air pressure will increase until it reaches a sufficient value for the air to escape by bubbling. Moisture profiles obtained considering two-phase flow was found a little bit delayed in comparison with that of one-phase flow (Fig. 8).

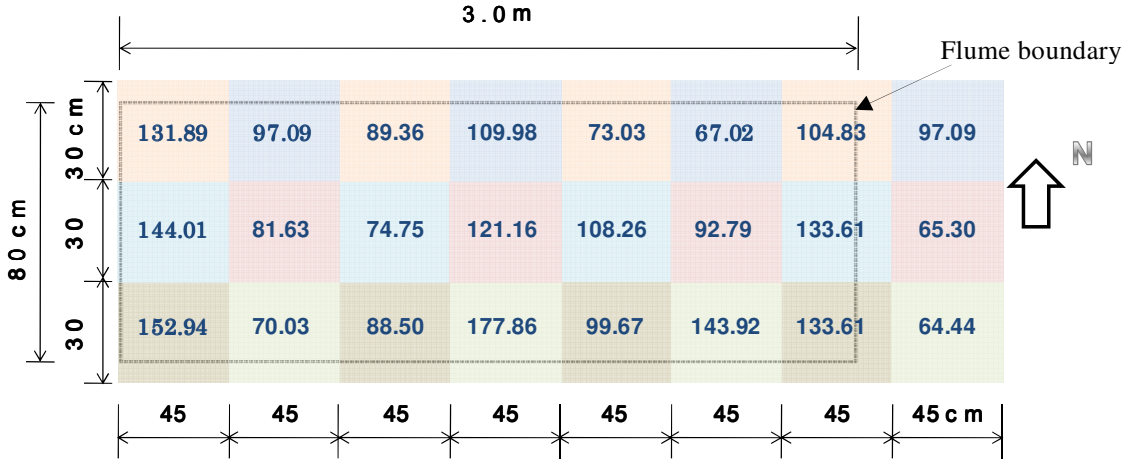

Fig. 6 Distribution of rainfall intensity (in mm/hr) over the flume

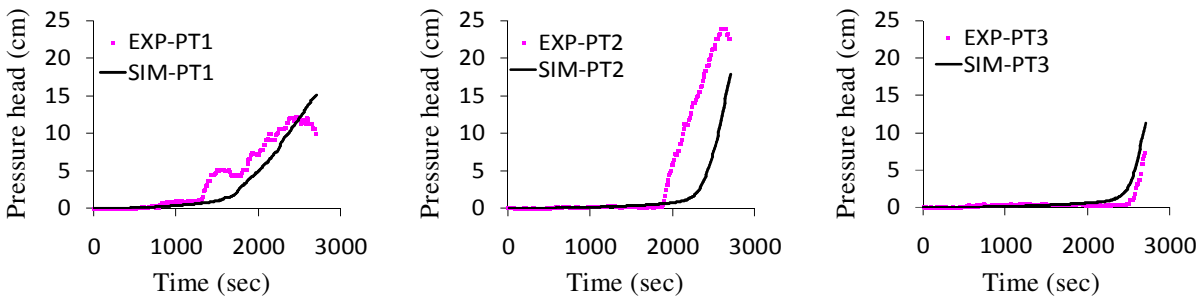

Fig. 7 Experimental and simulated air pressure head profiles

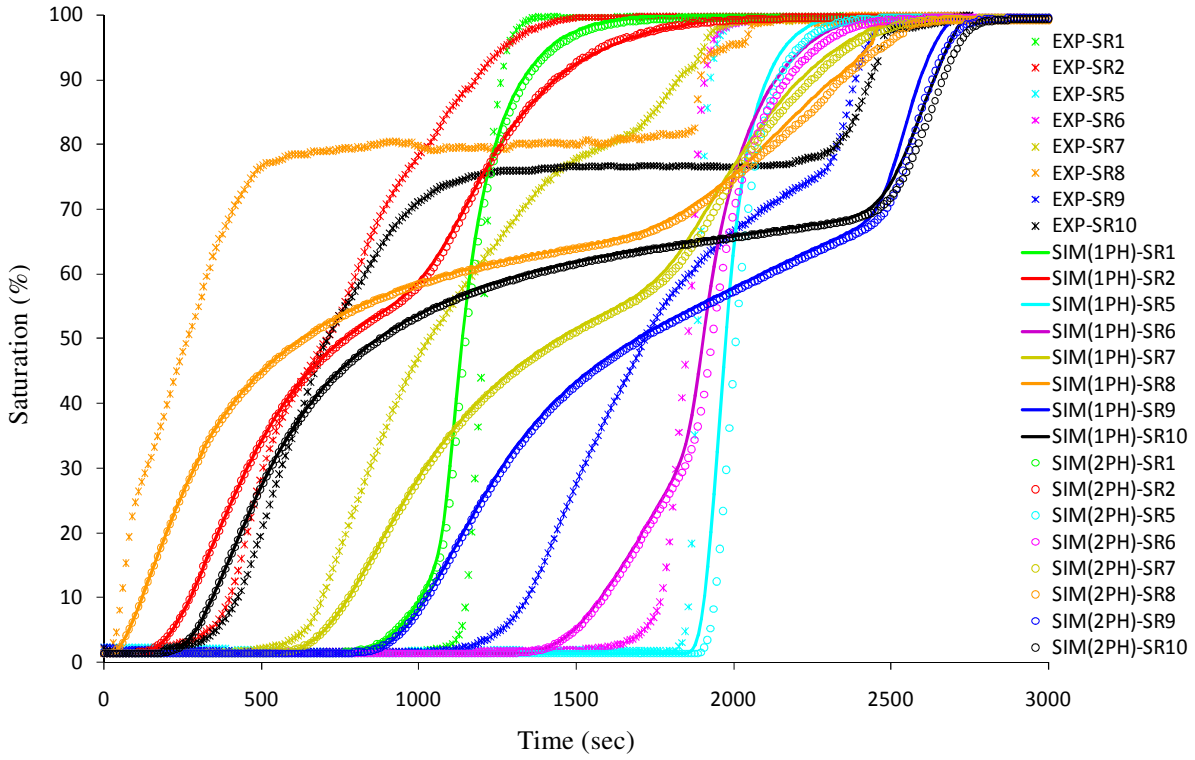

Fig. 8 Experimental and simulated moisture profiles

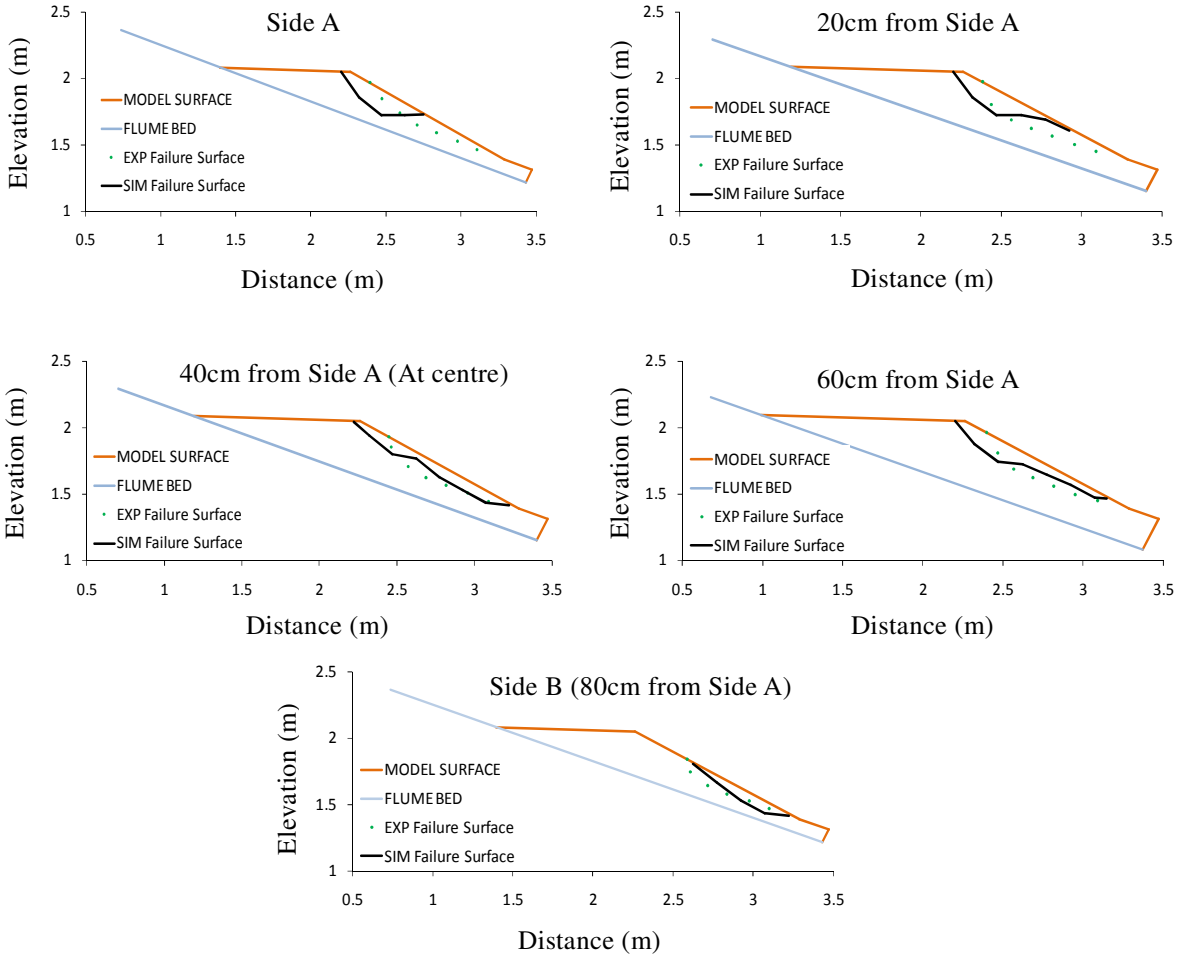

Fig. 9 Experimental and simulated critical slip surfaces (Time= 2780 second)

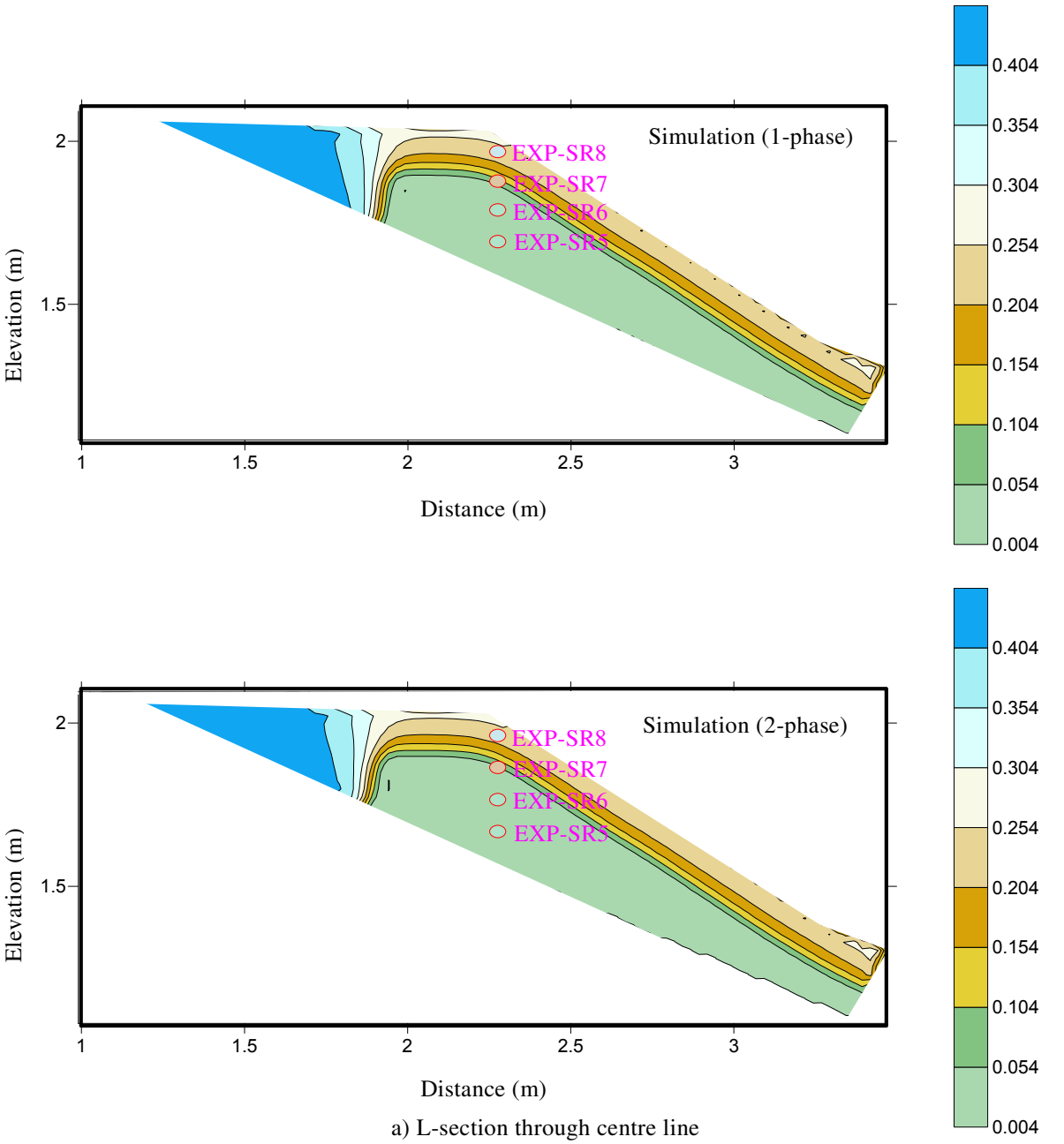

a) L-section through centre line

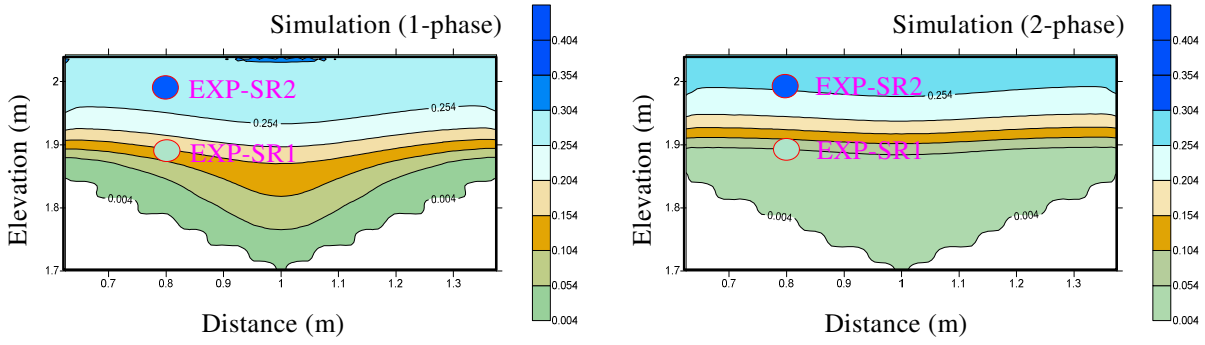

b) X-section through PR1

Fig. 10 Experimental and simulated moisture contents at 1100 second

In experiment the slope was failed at 2,780 second. Fig. 9 shows the comparison of experimental and simulated critical slip surfaces at 2780 second. In simulation calculated factor of safety was 0.737 in case of data obtained by one-phase as well as 2-phase seepage analysis. Simulated moisture content contour at 1,100 seconds is presented in Fig. 10. Experimental moisture contents observed by various profile probe sensors are also compared with simulated moisture contents in Fig. 10.

Janbu's simplified method only satisfies force equilibrium for the entire sliding mass and assumes resultant inter-slice forces horizontal where as it does not satisfy moment equilibrium. Also the assumption of horizontal resultant inter-slice forces does not represent its line of action indeed. For the same critical surface factor of safety obtained by other methods that also satisfying moment equilibrium will be higher.

5. Conclusions

In this study slope stability analysis was carried out using the pore water pressure and the moisture content calculated by three dimensional seepage flow model. Only a conventional water-phase seepage flow model as well as the water-air two-phase seepage flow model, coupled with two dimensional surface flow and erosion/deposition model, were used for seepage analysis. In seepage analysis, the influence of air on seepage was found to be less significant. More experimental studies are necessary to get experimental and simulated results quite close. The performance of the model can further be improved by incorporating more rigorous method of slope stability analysis.

Acknowledgements

The financial support provided by Japan Society for the Promotion of Science (JSPS) Grant-in-Aid for Scientific Research (B) 22360197(Hajime Nakagawa, Kyoto University) to this research is gratefully acknowledged.

References

Anderson, S.A. and Sitar, N. (1995): Analysis of rainfall-induced debris flow, Journal of Geotechnical Engineering, ASCE, Vol.121, No.7, pp.544-552.

Awal, R., Nakagawa, H., Kawaike, K., Baba, Y. and Zhang, H. (2009): Three dimensional transient seepage and slope stability analysis of landslide dam, Annuals of Disaster Prevention Research Institute, Kyoto University, No.52B, pp.689-696.

Baum, R.L., Savage, W.Z. and Godt, J.W. (2002): TRIGRS - a Fortran program for transient rainfall infiltration and grid-based regional slopestability analysis, Virginia, US Geological Survey, Open file report 02-424.

Borga, M., Fontana, G.D., De Ros, D. and Marchi L. (1998): Shallow landslide hazard assessment using a physically based model and digital elevation data, Environmental Geology, Vol.35, pp.81-88.

Brand, E.W. (1981): Some thoughts on rainfall induced slope failures, Proceedings of 10th International Conference on Soil Mechanics and Foundation Engineering, pp.373-376.

Brand, E.W. (1984): Landslides in Southeast Asia: a state of the art report, In Proceedings of the 4th International Symposium on Landslides, Toronto, Canada, Vol.1, pp.377- 384.

Brenner, R.P., Tam, H.K. and Brand, E.W. (1985): Field stress path simulation of rain-induced slope failure, Proceedings of 11th International Conference on Soil Mechanics and Foundation Engineering, Vol.2, pp.373-376.

Corominas, J. (2001): Landslides and Climate, Keynote Lectures from the 8th International Symposium on Landslides, Vol.4, pp.1-33.

Crosta, G.B. and Frattini, P. (2003): Distributed modeling of shallow landslides triggered by intense rainfall, Nat Haz Earth Syst Sci, Vol.3, pp.81-93.

Crozier, M. J. (1999): Prediction of rainfall-triggered landslides: a test of the Antecedent Water Status Model, Earth Surface Processes and Landforms, Vol.24, pp.825-833.

Dakshanamurthy, V., Fredlund, D.G. and Rahardjo, H (1984): Coupled three dimensional consolidation theory of unsaturated porous media, Proceedings of the fifth international conference on expansive soils, Adelaide, South Australia.

Dam, J.C. van and Feddes, R.A. (2000): Numerical simulation of infiltration, evaporation and shallow groundwater levels with the Richards equation, Journal of Hydrology, Vol.233, pp72-85.

Day, P. R. and Luthin, J. N. (1956): A numerical solution of the differential equation of flow for a vertical drainage problem, *Proceedings*, Soil Science Society of America, Vol. 20, pp. 443-447.

D'Odorico, P., Fagherazzi, S. and Rigon, R. (2005): Potential for landsliding: dependence on hyetograph characteristics, J Geophys Res Earth Surf 110(F1).

Frattini, P., Crosta, G.B., Fusi, N. and Negro, P.D. (2004): Shallow landslides in pyroclastic soil: a distributed modeling approach for hazard assessment, Engineering Geology, Vol.73, pp.277-295.

Fredlund, D.G., Morgenstern, N.R. and Widger, R.A. (1978): The shear strength of unsaturated soils, Canadian Geotechnical Journal, Vol.15, pp.313-321.

Fredlund, D.G. and Rahardjo, H. (1993): Soil mechanics for unsaturated soils, John Wiley and Sons Inc., 517.

Freeze, R.A. (1969): The mechanism of natural groundwater recharge and discharge 1. One-dimensional, vertical, unsteady, unsaturated flow above a recharging and discharging groundwater flow system, Water Resources Research, Vol.5, pp.153-171.

Freeze, R.A. (1971a): Three dimensional transient, saturated unsaturated flow in a groundwater basin, Water Resour. Res., Vol.7, pp.347-366.

Freeze, R.A. (1971b): Influence of the unsaturated flow domain on seepage through earth dams, Water Resour. Res., Vol.7, pp.929-941.

Freeze, R. A. (1978): Mathematical models of hillslope hydrology, in Kirkby, M. J., ed., Hillslope Hydrology, John Wiley, pp. 177-225.

Fukuzono, T. (1987): Experimental study of slope failure caused by heavy rainfall, Erosion and Sedimentation in the Pacific Rim, Proceedings of the Corvallis Symposium, August.

Griffiths, D.V. and Lu, N. (2005): Unsaturated slope stability analysis with steady infiltration or evaporation using elasto-plastic finite elements, Int. J. Numer. Anal. Meth. Geomech., Vol.29, pp.249-267.

Iverson, R. M. (2000): Landslide triggering by rainfall infiltration, Water Resources Research, Vol.36, pp.1987-1910.

Johnson, K. A. and Sitar, N. (1990): Hydrologic conditions leading to debris-flow initiations, Canadian Geotechnical Journal, Vol.27, pp.789-801.

Keim, R.F. and Skaugset, A.E. (2003): Modelling effects of forest canopies on slope stability, Hydrol Process, Vol.17, Vol.1457-1467.

Kirkby, M.J. (1978): Hillslope Hydrology, John Wiley & Sons, 389 pp.

Lan, H.X., Lee, C.F., Zhou, C.H. and Martin, C.D. (2005): Dynamic characteristics analysis of shallow landslides in response to rainfall event using GIS, Environmental Geology, Vol.47, pp.254-267.

Montgomery, D.R. and Dietrich, W.E. (1994): A physically based model for the topographic control on shallow landslide, Water Resources Research, Vol.30, pp.83-92.

Mukhlisin, M. and Taha, M.R. (2009): Slope Stability Analysis of a Weathered Granitic Hillslope as Effects of Soil Thickness, European Journal of Scientific Research, Vol.30, No.1, pp.36-44.

Nakagawa, H., Takahashi, T., Satofuka, Y. and Kawaike, K. (2003): Numerical simulation of sediment disasters caused by heavy rainfall in Camuri Grande basin, Venezuela 1999, Proceedings of the Third Conference on Debris-Flow Hazards Mitigation: Mechanics, Prediction, and Assessment, Switzerland, Rotterdam, pp.671-682.

Ng, C.W.W. and Shi, Q. (1998): A numerical investigation of the stability of unsurated soil slopes subjected to transient seepage, Computers and Geotechnics, Vol.22, No.1, pp.1-28.

Rahardjo, H., Lim, T.T., Chang, M.F. and Fredlund, D.G. (1995): Shear strength characteristics of a residual soil, Canadian Geotechnical Journal, Vol.32, pp.60-77.

Richards, L.A. (1931): Capillary conduction of liquids in porous mediums, Physics, Vol.1, pp.318-333.

Sanderson, F., Bakkehoi, S., Hestenes, E., and Lied, K. (1996): The influence of meteorological factors on the initiation of debris flows, rockfalls,

rockslides and rockmass stability, in: Landslides. Proceedings 7th International Symposium on Landslides, edited by: Senneset, K., A.A. Balkema.

Sassa, K. (1972): Analysis on slope stability: I, Mainly on the basis of the indoor experiments using the standard sand produced in Toyoura, Japan, Journal of the Japan Society of Erosion Control Engineering, Vol.25, No.2, pp.5-17 (in Japanese with English abstract).

Sassa, K. (1974): Analysis on slope stability: II, Mainly on the basis of the indoor experiments using the standard sand produced in Toyoura, Japan, Journal of the Japan Society of Erosion Control Engineering, Vol.26, No.3, pp.8-19 (in Japanese with English abstract).

Sharma, R.H. (2006): Study on integrated modeling of rainfall induced sediment hazards, Doctoral Thesis, Kyoto University.

Sidle, R.C. and Swanston, D.N. (1982): Analysis of a small debris slide in coastal Alaska, Canadian Geotechnical Journal, Vol.19, pp.167-174.

Sitar, N., Anderson, S.A. and Johnson, K.A. (1992): Conditions leading to the initiation of rainfall-induced debris flows, Proceedings of the Journal of the Geotechnical Engineering Division Specialty Conference on Stability and Performance of Slopes and Embankments-II, ASCE, New York, NY, pp.834-839.

Takahashi T. (1991): Debris flow, Monograph Series of IAHR, Balkema, pp.1-165.

Takahashi, T. and Nakagawa, H. (1994): Flood/debris flow hydrograph due to collapse of natural dam by overtopping, Journal of Hydroscience and Hydraulic Engineering, JSCE, Vol.12, No.2, pp.41-49.

Terlien, M. T. J. (1998): The determination of statistical and deterministic hydrological landslide-triggering thresholds, Environmental Geology, Vol.35, pp.2-3.

Terzaghi, K. (1950): Mechanism of landslides, In: Paige, S. (Ed.), Application of Geology to Engineering Practice (Berkey Volume), Geological Society of America, New York, pp.83-123.

Toll, D.G. (2001): Rainfall-induced landslides in Singapore, Proc. Institution of Civil Engineers, Geotechnical Engineering, Vol.149, No.4, pp.211-16.

Touma, J. and Vauclin, M. (1986): Experimental and numerical analysis of two-phase infiltration in a partially saturated soil, Transport in Porous Media, Vol.1, pp.27-55.

Tsai, T.L. and Yang, J.C. (2006): Modeling of rainfall-triggered shallow landslide, Environmental Geology, Vol.50, No.4, pp.525-534.

Tsai, T.L. (2007): The influence of rainstorm pattern on shallow landslide, Environmental Geology.

Tsai, T.L., Chen, H.E. and Yang, J.C. (2008): Numerical modeling of rainstorm-induced shallow landslides in saturated and unsaturated soils, Environmental Geology, Vol.55, pp.1269-1277.

Tsutsumi, D. and Fujita, M. (2008):Relative importance of slope material properties and timing of rain fall for the occurance of landslides, International Journal of Erosion Control Engineering, Vol.1, No.2.

van Genuchten, M. T. (1980): A closed-form equation for predicting the hydraulic conductivity of unsaturated soils, Soil Sci. Soc. Amer. J., Vol.48, pp.703-708.

Vasconcellos, C. A. B. de and Amorim,J. C. C. (2001): Numerical simulation of unsaturated flow in porous media using a mass conservative model, em “Proceeding of COBEM. 2001, Fluid Mechanics”, Vol.8, pp.139-148, Uberlândia, MG.

Wang, G. and Sassa, K. (2003): Pore-pressure generation and movement of rainfall-induced landslides; effects on grain size and fine-particle content, Journal of Engineering Geology, Vol.69, pp.109-125.

Wieczorek, G. F. (1987): Effect of rainfall intensity and duration on debris flows in central Santa Cruz Mountains, California, Geolog. Soc. Amer., Reviews in Engineering Geology, Vol.7.

Wu, W. and Slide, R.C. (1995): A distributed slope stability model for steep forested basins, Water Resources Research, Vol.31, pp.2097-2110.

降雨による斜面崩壊に関する実験及び数値解析

Ram Krishna REGMI*・中川一・川池健司・馬場康之・張浩

*京都大学大学院工学研究科

要　旨

本研究は，降雨による斜面崩壊を予測することを目的としている。実験と数値解析により斜面崩壊のメカニズムについて検討を行った。間隙水圧と含水量を解く３次元浸透流解析によって斜面の安定解析を実施した。従来の水相のみの浸透流だけでなく，水と空気の２相を解析する浸透流モデルを２次元の表層流および浸食/堆積モデルとカップリングし，実験へ適用し検証を行った。数値解析により，浸透流と斜面安定において間隙内の空気の影響は小さく，２相で解析する必要性が低いことが示された。

キーワード：浸透流解析，飽和土，斜面安定，表層崩壊